

# NON-MINIMALLY GRAVITY-COUPLED INFLATIONARY MODELS

**C. PALLIS**

*Department of Physics, University of Cyprus,  
P.O. Box 20537, CY-1678 Nicosia, CYPRUS  
kpallis@auth.gr*

## ABSTRACT

We consider the non-supersymmetric models of chaotic (driven by a quadratic potential) and hybrid inflation, taking into account the minimal possible radiative corrections to the inflationary potential. We show that two simple coupling functions  $f(\sigma)$  (with a parameter  $c_{\mathcal{R}}$  involved) between the inflaton field  $\sigma$  and the Ricci scalar curvature ensure, for sub-Planckian values of the inflaton field, observationally acceptable values for the spectral index,  $n_s$ , and sufficient reheating after inflation. In the case of chaotic inflation we consider two models with large  $c_{\mathcal{R}}$ 's resulting to  $n_s \simeq 0.955$  or  $0.967$  and tensor-to-scalar ratio  $r \simeq 0.2$  or  $0.003$ , respectively. In the case of hybrid inflation, the selected  $f(\sigma)$  assists us to obtain hilltop-type inflation. For values of the relevant mass parameter,  $m$ , less than  $10^6$  TeV and the observationally central value of  $n_s$ , we find  $c_{\mathcal{R}} \simeq (0.015 - 0.078)$  with the relevant coupling constants  $\lambda = \kappa$  and the symmetry breaking scale,  $M$ , confined in the ranges  $(2 \cdot 10^{-7} - 0.001)$  and  $(1 - 16.8) \cdot 10^{17}$  GeV, respectively.

## 1 INTRODUCTION

*Non-minimal inflation* (non-MI) [1] i.e. inflation constructed in the presence of a non-minimal coupling between the inflaton field and the Ricci scalar curvature,  $\mathcal{R}$ , has gained a fair amount of recent attention [2–4]. In particular, it is shown that non-MI can be realized within the *Standard Model* (SM) – or minimal extensions [5] of it – provided the inflaton couples strongly enough to  $\mathcal{R}$ . The role of inflaton can be played either by the Higgs doublet either by a SM singlet coupled to Higgs. Although quite compelling, non-MI within SM suffers from (i) several computational uncertainties regarding the impact of the quantum corrections in the presence of such a strong non-minimal gravitational coupling and (ii) the ambiguity about the hierarchy between the cutoff scale of the effective theory and the energy scale of the inflationary plateau [6, 7]. Be that as it may, it would be interesting to examine if appropriately selected non-minimal gravitational couplings can have beneficial consequences – as for the reconstruction of the cosmic expansion history [8] – for other well-motivated and rather natural models of inflation (for a survey see, e.g., Ref. [9]).

Two such models are undoubtedly *Chaotic* (CI) [10] and *Hybrid Inflation* (HI) [11]. In this paper we focus on the non-supersymmetric version of these models. CI driven by a quadratic potential provides the simplest realization of inflation without initial-value problem and with quite interesting predictions for the (scalar) spectral index,  $n_s$ , and the scalar-to-tensor ratio,  $r$ . However, trans-Planckian inflaton-field values are typically required to allow for a sufficiently long period of inflation. Thus non-renormalizable corrections from quantum gravity are expected to destroy the flatness of the potential, invalidating thereby CI. On the other hand, HI – although can be accommodated with sub-Planckian values for the inflaton – suffers from the problem of the enhanced  $n_s$  which turns out to be, mostly, well above the prediction of the fitting [12] of the five-year results from the *Wilkinson Microwave Anisotropy Probe Satellite* (WMAP5) plus *baryon-acoustic-oscillations* (BAO) and *supernovae* (SN) data – for an up-to-date analysis of the problem of initial conditions within HI, see Ref. [13].

**CONTENTS**

<b>1</b>	<b>INTRODUCTION</b>	<b>1</b>
<b>2</b>	<b>INFLATION WITH NON-MINIMAL GRAVITATIONAL COUPLING</b>	<b>2</b>
2.1	NON-MINIMALLY CURVATURE-COUPLED SCALAR THEORY . . . . .	3
2.2	INFLATIONARY OBSERVABLES – CONSTRAINTS . . . . .	3
<b>3</b>	<b>NON-MINIMAL CHAOTIC INFLATION</b>	<b>5</b>
3.1	RESULTS FOR MCI . . . . .	5
3.2	RESULTS FOR NON-MCI . . . . .	6
<b>4</b>	<b>NON-MINIMAL HYBRID INFLATION</b>	<b>9</b>
4.1	RESULTS FOR MHI . . . . .	10
4.2	RESULTS FOR NON-MHI . . . . .	12
<b>5</b>	<b>CONCLUSIONS</b>	<b>15</b>
	<b>REFERENCES</b>	<b>16</b>

Note, in passing, that the introduction of *supersymmetry* (SUSY) and its local extension – supergravity (SUGRA) – can alleviate the shortcomings of both models – see Ref. [14] for several resolutions to the problem of CI and Ref. [15–19] for proposals related to the disadvantage of HI. However, we have to accept that there is no direct experimental confirmation of SUSY until now. On the contrary, there is a strong observational evidence in favor of the inflationary paradigm. Consequently, it is worthwhile to build models of CI and HI consistently with the observations, even without the presence of SUSY – for similar recent attempts, see Ref. [20, 21].

In this paper, we propose two types of non-minimal coupling functions  $f(\sigma)$  between the inflaton and  $\mathcal{R}$  which support a resolution to the aforementioned problems of CI and HI. After the end of non-MI, both  $f(\sigma)$ 's shrink to unit assuring thereby, a safe transition to the Einstein gravity in time. In the case of *non-minimal CI* (non-MCI), two models with clearly distinctive results are investigated. In the case of *non-minimal HI* (non-MHI), the inflationary trajectory is concave downwards and so, inflation turns out to be of hilltop-type [22]. In both cases, the minimal possible radiative corrections [23] to the inflationary potential are considered, sub-Planckian values of the inflaton field are required and adequate reheating of the universe is accomplished via curvature-induced [24] couplings of the inflaton to matter fields. Comparisons with the results obtained for the minimal version of both inflationary models are also displayed.

Below, we describe the generic formulation of non-MI (Sec. 2) and then apply the relevant results, for appropriate choices of  $f(\sigma)$ , in the case of non-MCI and non-MHI in Sec. 3 and 4 respectively. Finally, Sec. 5 summarizes our conclusions. Throughout the text, we set natural units for the Planck's constant, Boltzmann's constant and the velocity of light ( $\hbar = c = k_B = 1$ ) the subscript  $\chi$  denotes derivation *with respect to* (w.r.t.) the field  $\chi$  (e.g.,  ${}_{,\chi\chi} = d^2/d\chi^2$ ) and a bar over a field  $\chi$  denotes normalization w.r.t the reduced Planck mass,  $m_P = 2.44 \cdot 10^{18}$  GeV, i.e.,  $\bar{\chi} = \chi/m_P$ . Finally, we follow the conventions of Ref. [25] for the quantities related to the gravitational sector of our set-up.

**2 INFLATION WITH NON-MINIMAL GRAVITATIONAL COUPLING**

Non-MI, by its definition, can be realized by a scalar field non-minimally coupled to Ricci scalar curvature. The formulation of a such theory is described in Sec. 2.1. Based on it, we then derive the inflationary observables and impose observational constraints in Sec. 2.2.

### 2.1 NON-MINIMALLY CURVATURE-COUPLED SCALAR THEORY

The dynamics of a scalar field  $\sigma$  non-minimally coupled to  $\mathcal{R}$  through a coupling function  $f(\sigma)$  is controlled, in the Jordan frame, by the following action – see, e.g., Ref. [4]:

$$\mathcal{S} = \int d^4x \sqrt{-g} \left( -\frac{1}{2} m_{\text{P}}^2 f(\sigma) \mathcal{R} + \frac{1}{2} g^{\mu\nu} \partial_\mu \sigma \partial_\nu \sigma - V(\sigma) \right), \quad (2.1)$$

where  $g$  is the determinant of the background Friedmann-Robertson-Walker metric [25]. To guarantee the validity of the ordinary Einstein gravity at low energy, we require  $f(\langle\sigma\rangle) = 1$ , where  $\langle\sigma\rangle$  is the *vacuum expectation value* (v.e.v) of  $\sigma$  at the end of non-MI.

The action in Eq. (2.1) can be brought in a simpler form by performing a conformal transformation [26] to the so-called Einstein frame where the the gravitational sector of our model becomes minimal. Indeed, if we define the Einstein-frame metric

$$\hat{g}_{\mu\nu} = f g_{\mu\nu} \Rightarrow \begin{cases} \sqrt{-\hat{g}} = f^2 \sqrt{-g} \text{ and } \hat{g}^{\mu\nu} = g^{\mu\nu} / f, \\ \hat{\mathcal{R}} = (\mathcal{R} + 3\Box \ln f + 3g^{\mu\nu} \partial_\mu f \partial_\nu f / 2f^2) / f \end{cases} \quad (2.2)$$

– where  $\Box = (-g)^{-1/2} \partial_\mu (\sqrt{-g} \partial^\mu)$  and hat is used to denote quantities defined in the Einstein frame – and introduce the Einstein-frame canonically normalized field,  $\hat{\sigma}$ , and potential,  $\hat{V}$ , defined as follows:

$$\left( \frac{d\hat{\sigma}}{d\sigma} \right)^2 = J^2 = \frac{1}{f} + \frac{3}{2} m_{\text{P}}^2 \left( \frac{f, \sigma}{f} \right)^2 \quad \text{and} \quad \hat{V}(\hat{\sigma}) = \frac{V(\hat{\sigma}(\sigma))}{f(\hat{\sigma}(\sigma))^2}, \quad (2.3)$$

the action in Eq. (2.1) can be simplified, taking the form

$$\mathcal{S} = \int d^4x \sqrt{-\hat{g}} \left( -\frac{1}{2} m_{\text{P}}^2 \hat{\mathcal{R}} + \frac{1}{2} \hat{g}^{\mu\nu} \partial_\mu \hat{\sigma} \partial_\nu \hat{\sigma} - \hat{V}(\hat{\sigma}) \right). \quad (2.4)$$

Based on the action above, we can proceed readily to the analysis of non-MI in the Einstein frame using the standard slow-roll approximation [9, 27] – see below. It can be shown [28] that the results calculated this way are the same as if we had calculated them with the non-minimally coupled scalar field in the Jordan frame.

One of the outstanding features of the scalar theories with non-minimal  $f(\sigma)$  is that  $\sigma$  can decay via gravitational effects [24] even without explicit couplings between  $\sigma$  and matter fields. This is, because couplings arise spontaneously when  $\sigma$  settles in its v.e.v,  $\langle\sigma\rangle$ , and oscillates, with coupling constants involving derivatives of  $f(\sigma)$  calculated for  $\sigma = \langle\sigma\rangle$ . If we identify  $\sigma$  as the inflaton, these couplings can ensure the reheating of the universe. Assuming the existence of a bosonic field minimally coupled to gravity, with negligible mass compared to the mass of  $\sigma$ ,  $m_\sigma = V_{,\sigma\sigma}(\langle\sigma\rangle)^{1/2}$ , we get [24, 29] for the reheat temperature

$$T_{\text{rh}} \simeq \left( \frac{5\pi^2 g_{\rho*}(T_{\text{rh}})}{72} \right)^{-1/4} \sqrt{\Gamma_\sigma m_{\text{P}}} \quad \text{where} \quad \Gamma_\sigma \simeq \frac{f_{,\sigma}(\langle\sigma\rangle)^2 m_\sigma^3}{128\pi} \left( 1 + \frac{3}{2} m_{\text{P}}^2 f_{,\sigma}(\langle\sigma\rangle)^2 \right)^{-1} \quad (2.5)$$

is the decay rate of  $\sigma$ , in the regime  $T \ll m_\sigma$  which is valid in our applications. Clearly, this construction is applicable if  $f_{,\sigma}(\langle\sigma\rangle) \neq 0$  (and this is valid for the  $f(\sigma)$ 's considered in Sec. 3 and 4). Also, assuming the particle spectrum of SM, we set  $g_{\rho*} = 106.75$  for the relativistic degrees of freedom.

### 2.2 INFLATIONARY OBSERVABLES – CONSTRAINTS

Under the assumption that (i) the curvature perturbations generated by  $\sigma$  is solely responsible for the observed curvature perturbation and (ii) there is a conventional cosmological evolution (see below) after inflation, the inflationary parameters can be restricted imposing the following requirements:

(a) The power spectrum  $P_{\mathcal{R}}$  of the curvature perturbations generated by  $\sigma$  at the pivot scale  $k_* = 0.002/\text{Mpc}$  is to be confronted with the WMAP5 data [12],

$$P_{\mathcal{R}}^{1/2} = \frac{1}{2\sqrt{3}\pi m_{\text{P}}^3} \frac{\widehat{V}(\widehat{\sigma}_*)^{3/2}}{|\widehat{V}_{,\widehat{\sigma}}(\widehat{\sigma}_*)|} = \frac{|J(\sigma_*)|}{2\sqrt{3}\pi m_{\text{P}}^3} \frac{\widehat{V}(\sigma_*)^{3/2}}{|\widehat{V}_{,\sigma}(\sigma_*)|} \simeq 4.91 \cdot 10^{-5}, \quad (2.6)$$

where  $\sigma_* [\widehat{\sigma}_*]$  is the value of  $\sigma [\widehat{\sigma}]$  when  $k_*$  crosses outside the inflationary horizon.

(b) The number of e-foldings,  $\widehat{N}_*$ , that the scale  $k_*$  suffers during FHI is to account for the total number of e-foldings  $\widehat{N}_{\text{tot}}$  required for solving the horizon and flatness problems of standard big bag cosmology, i.e.,  $\widehat{N}_* = \widehat{N}_{\text{tot}}$ . Specifically, we calculate  $\widehat{N}_*$  through the relation

$$\widehat{N}_* = \frac{1}{m_{\text{P}}^2} \int_{\widehat{\sigma}_{\text{f}}}^{\widehat{\sigma}_*} d\widehat{\sigma} \frac{\widehat{V}}{\widehat{V}_{,\widehat{\sigma}}} = \frac{1}{m_{\text{P}}^2} \int_{\sigma_{\text{f}}}^{\sigma_*} d\sigma J^2 \frac{\widehat{V}}{\widehat{V}_{,\sigma}}, \quad (2.7)$$

where  $\sigma_{\text{f}} [\widehat{\sigma}_{\text{f}}]$  is the value of  $\sigma [\widehat{\sigma}]$  at the end of inflation, which can be found, in the slow-roll approximation and for the considered in this paper models, from the condition

$$\max\{\widehat{\epsilon}(\sigma_{\text{f}}), |\widehat{\eta}(\sigma_{\text{f}})|\} = 1, \quad \text{where}$$

$$\widehat{\epsilon} = \frac{m_{\text{P}}^2}{2} \left( \frac{\widehat{V}_{,\widehat{\sigma}}}{\widehat{V}} \right)^2 = \frac{m_{\text{P}}^2}{2J^2} \left( \frac{\widehat{V}_{,\sigma}}{\widehat{V}} \right)^2 \quad \text{and} \quad \widehat{\eta} = m_{\text{P}}^2 \frac{\widehat{V}_{,\widehat{\sigma}\widehat{\sigma}}}{\widehat{V}} = \frac{m_{\text{P}}^2}{J^2} \left( \frac{\widehat{V}_{,\sigma\sigma}}{\widehat{V}} - \frac{\widehat{V}_{,\sigma}}{\widehat{V}} \frac{J_{,\sigma}}{J} \right). \quad (2.8)$$

The required  $\widehat{N}_{\text{tot}}$  at  $k_*$  can be easily derived [19] consistently with our assumption of a conventional post-inflationary evolution. In particular, we assume that inflation is followed successively by the following three epochs: (i) the decaying-inflaton dominated era which lasts at a reheat temperature  $T_{\text{rh}}$ , (ii) a radiation dominated epoch, with initial temperature  $T_{\text{rh}}$ , which terminates at the matter-radiation equality, (iii) the matter dominated era until today. In particular, we obtain – c.f. Ref. [19]

$$\widehat{N}_{\text{tot}} \simeq 22.4 + 2 \ln \frac{V(\sigma_*)^{1/4}}{1 \text{ GeV}} - \frac{4}{3} \ln \frac{V(\sigma_{\text{f}})^{1/4}}{1 \text{ GeV}} + \frac{1}{3} \ln \frac{T_{\text{rh}}}{1 \text{ GeV}} + \frac{1}{2} \ln \frac{f(\sigma_{\text{f}})}{f(\sigma_*)}, \quad (2.9)$$

where the last term emerges [7] from the transition from the Jordan to Einstein frame. Note that  $\widehat{R} = \sqrt{f}R$  with  $R$  being the scale factor of the universe.

(c) The (scalar) spectral index,  $n_{\text{s}}$ , its running,  $a_{\text{s}}$ , and the scalar-to-tensor ratio  $r$  are to be consistent with the fitting [12] of the WMAP5 plus BAO and SN data, i.e.,

$$(a) \ n_{\text{s}} = 0.96 \pm 0.026, \quad (b) \ -0.068 \leq a_{\text{s}} \leq 0.012 \quad \text{and} \quad (c) \ r < 0.22, \quad (2.10)$$

at 95% confidence level (c.l.). The observable quantities above can be estimated through the relations:

$$n_{\text{s}} = 1 - 6\widehat{\epsilon}_* + 2\widehat{\eta}_*, \quad \alpha_{\text{s}} = \frac{2}{3} (4\widehat{\eta}_*^2 - (n_{\text{s}} - 1)^2) - 2\widehat{\xi}_* \quad \text{and} \quad r = 16\widehat{\epsilon}_*, \quad (2.11)$$

where  $\widehat{\xi} = m_{\text{P}}^4 \widehat{V}_{,\widehat{\sigma}} \widehat{V}_{,\widehat{\sigma}\widehat{\sigma}} / \widehat{V}^2 = m_{\text{P}}^2 \widehat{V}_{,\sigma} \widehat{\eta}_{,\sigma} / \widehat{V} J^2 + 2\widehat{\eta}\widehat{\epsilon}$  and the variables with subscript  $*$  are evaluated at  $\sigma = \sigma_*$ . Note, in passing, that the utilized here non minimal  $f(\sigma)$ 's do not produce [30] observationally interesting non-gaussianity – for reviews see, e.g., Ref. [31].

(d) To avoid corrections from quantum gravity, we impose two additional theoretical constraints on our models – keeping in mind that  $\widehat{V}(\sigma_{\text{f}}) \leq \widehat{V}(\sigma_*)$ :

$$(a) \ \widehat{V}(\sigma_*)^{1/4} \leq m_{\text{P}} \quad \text{and} \quad (b) \ \sigma_* \leq m_{\text{P}}. \quad (2.12)$$

Although it is argued [20, 32] that violation of Eq. (2.12b) may not be necessarily fatal, we insist on imposing this condition in order to deliberate our proposal from our ignorance about the Planck-scale physics. To be even more conservative, we have to check the hierarchy between the ultraviolet cut-off,

$\Lambda$ , of the effective theory and the inflationary scale. The former can be found from the non-renormalizable terms arising in Eq. (2.4), whereas the latter is represented by  $\widehat{V}(\sigma_*)^{1/4}$  or, less restrictively, by the corresponding Hubble parameter,  $\widehat{H}_* = \widehat{V}(\sigma_*)^{1/2}/\sqrt{3}m_{\text{P}}$ . In particular, the validity of the effective theory implies [6]

$$(a) \widehat{V}(\sigma_*)^{1/4} \leq \Lambda \quad \text{or} \quad (b) \widehat{H}_* \leq \Lambda. \quad (2.13)$$

This requirement applies mainly in cases where the involved in  $f(\sigma)$  constant  $c_{\mathcal{R}}$  takes relatively large values – as for SM non-MI [2–4] – jeopardizing, thereby, the validity of the classical approximation, on which the analysis of the inflationary behavior in this section is based.

### 3 NON-MINIMAL CHAOTIC INFLATION

We focus on CI driven primarily by a quadratic potential of the form

$$V = \frac{1}{2}m^2\sigma^2 + V_{\text{rc}} \quad \text{where} \quad V_{\text{rc}} = \frac{1}{64\pi^2}m^4 \ln \frac{m^2}{Q^2} \quad (3.1)$$

are radiative corrections [23] to the inflationary potential. The bulk of our results – see Sec. 3.2 – are independent of the renormalization scale,  $Q$ , which is set equal to  $m_{\text{P}}$ . We below recall (Sec. 3.1) the results for MCI (with  $f(\sigma) = 1$ ) and describe (Sec. 3.2) our findings for non-MCI, adopting the following coupling function – recall that  $\bar{\sigma} = \sigma/m_{\text{P}}$ :

$$f(\sigma) = (1 + c_{\mathcal{R}}\bar{\sigma})^{-n} \quad \text{with} \quad n = \pm 1. \quad (3.2)$$

Note, in passing, that results for non-MCI with quartic potential ( $V = \lambda\sigma^4/4!$ ) are presented in Ref. [1, 33, 34]. The inflationary scenario based on this potential with  $f(\sigma) = 1$  seems to be excluded [12, 20] due to the enhanced predicted  $r$ . As we explicitly verified, if we employ the standard non-minimal coupling function,  $f(\sigma) = 1 + c_{\mathcal{R}}\bar{\sigma}^2$ , with  $80 \lesssim c_{\mathcal{R}} \lesssim 300$  and  $0.2 \lesssim \lambda/10^{-4} \lesssim 3$  – c.f. Ref. [33, 34] – we can rescue the model consistently with the constraints of Sec. 2.2 for an indicative  $T_{\text{rh}} = 10^{10}$  GeV. In particular the lower [upper] bound of the allowed regions of  $c_{\mathcal{R}}$  and  $\lambda$  comes from Eq. (2.12b) [Eq. (2.13a) with  $\Lambda = m_{\text{P}}/c_{\mathcal{R}}$ ]. Note, however, that the standard non-trivial  $f(\sigma)$  does not support reheating along the lines of Eq. (2.5).

#### 3.1 RESULTS FOR MCI

For MCI the slow-roll parameters and the number of  $e$ -foldings suffered from  $k_*$  can be calculated applying Eq. (2.8) and Eq. (2.7) – after removing hats and setting  $J = 1$  – with results

$$\epsilon = \eta = 2/\bar{\sigma}^2 \quad \text{and} \quad N_* = (\bar{\sigma}_*^2 - \bar{\sigma}_{\text{f}}^2)/4. \quad (3.3)$$

Using these results, imposing the condition of Eq. (2.8) and employing Eq. (2.11) we can derive

$$\bar{\sigma}_{\text{f}} = \sqrt{2}, \quad \bar{\sigma}_* \simeq 2\sqrt{N_*}, \quad n_{\text{s}} \simeq 1 - 2/N_* \quad \text{and} \quad r \simeq 8/N_*. \quad (3.4)$$

Clearly trans-Planckian values of  $\sigma$  are required and observationally favored  $n_{\text{s}}$  and  $r$  are obtained. More precisely, imposing the requirements (a) and (b) of Sec. 2.2 for several  $T_{\text{rh}}$ 's we get numerically the values of  $\sigma_*$ ,  $m$ ,  $n_{\text{s}}$ ,  $\alpha_{\text{s}}$  and  $r$  listed in Table 1 – c.f. Ref. [20]. As  $T_{\text{rh}}$  decreases,  $N_*$  decreases too – see Eq. (2.9) – and so,  $\sigma_*$  and  $n_{\text{s}}$  slightly decrease whereas  $r$  increases – see Eq. (3.4). The resulting  $n_{\text{s}}$ ,  $\alpha_{\text{s}}$  and  $r$  lie within the range of Eq. (2.10). In all cases, Eq. (2.12a) is valid whereas the upper bound of Eq. (2.12b) is surpassed.

$T_{\text{rh}}$ (GeV)	$\sigma_*/m_{\text{P}}$	$m$ ( $10^{13}$ GeV)	$n_{\text{s}}$	$\alpha_{\text{s}}$ ( $10^{-4}$ )	$r$
$10^{10}$	15.13	1.6	0.965	6.1	0.139
$10^6$	14.73	1.69	0.963	6.7	0.147
$10^5$	14.61	1.72	0.962	7	0.15
$10^4$	14.5	1.74	0.962	7.2	0.152

**Table 1:** Values of parameters allowed by Eqs. (2.6), (2.7) and (2.9) for MCI with several  $T_{\text{rh}}$ 's.

### 3.2 RESULTS FOR NON-MCI

From Eqs. (2.8), (3.3) and (3.4) we can infer that the amplitude of the inflaton field within non-MCI can become sub-Planckian if  $J \simeq 1/f(\sigma) \gg 1$  and  $\widehat{V}_{,\sigma}/\widehat{V} \simeq V_{,\sigma}/V$ . These two objectives can be achieved if we employ  $f(\sigma)$  given by Eq. (3.2) with  $n > 0$  and  $c_{\mathcal{R}} \gg 1$ . Another possibility would be to take  $f(\sigma) = \exp(-c_{\mathcal{R}}\bar{\sigma})$  with  $c_{\mathcal{R}} \sim 10$ . However, in the latter case the resulting  $r$  violates Eq. (2.10c) and therefore, this option can be declined. Similar problem arises also if we use  $n > 1$  – see Sec. 3.2.1. On the other hand, for  $n = -1$ ,  $\widehat{V}$  in Eq. (2.3b) becomes very flat for sufficiently large  $\bar{\sigma}$ 's and so, a new type of non-MCI can take place. Decreasing  $n$  for  $n < 0$  we find inflationary solutions, only for  $c_{\mathcal{R}} < 0.001$ , which break Eq. (2.12b). Similar conclusions are also drawn for the standard non-minimal  $f(\sigma)$  – see Ref. [33].

In our numerical code we use as input parameters  $m, \sigma_*, c_{\mathcal{R}}$  and  $n$ . For every chosen  $n$  and  $c_{\mathcal{R}}$  we restrict  $m$  and  $\sigma_*$  so as the conditions (a) and (b) of Sec. 2.2 – with  $T_{\text{rh}}$  evaluated consistently with Eq. (2.5) – are fulfilled. Our results for  $n = +1$  and  $n = -1$  are presented respectively in Fig. 1 and Fig. 2, where we draw the allowed values of  $m$  (solid line) and  $T_{\text{rh}}$  (dashed line) [ $\sigma_f$  (solid line) and  $\sigma_*$  (dashed line)] versus  $c_{\mathcal{R}}$  for non-MCI (a) [(b)]. For both  $n = \pm 1$ , satisfying Eq. (2.12b) gives a lower bound on  $c_{\mathcal{R}}$  – see Fig. 1-(b) and Fig. 2-(b). On the other hand, the upper bound on  $c_{\mathcal{R}}$  comes from Eq. (2.10c) for  $n = +1$  and from the fact that the enhanced resulting  $m$ 's destabilize the inflationary path through the radiative corrections in Eq. (3.1) for  $n = -1$ . From our data we also remark that the resulting  $m$ 's are almost two orders of magnitude lower [larger] than those obtained within MCI for  $n = +1$  [ $n = -1$ ]. These results depend, though very weakly, on  $\widehat{N}_{\text{tot}}$  and therefore, on the reheating mechanism – see Eq. (2.9). All in all, we obtain

$$625 \lesssim c_{\mathcal{R}} \lesssim 2.1 \cdot 10^7, \quad 47 \gtrsim \frac{m}{10^7 \text{ TeV}} \gtrsim 1.6 \quad \text{and} \quad 52 \gtrsim \widehat{N}_* \gtrsim 47.9, \quad \text{for } n = -1, \quad (3.5)$$

$$83 \lesssim c_{\mathcal{R}} \lesssim 3120, \quad 3 \lesssim \frac{m}{10^{12} \text{ TeV}} \lesssim 8.6 \quad \text{and} \quad 58.8 \lesssim \widehat{N}_* \lesssim 59.9, \quad \text{for } n = +1. \quad (3.6)$$

In both cases, the predicted  $n_{\text{s}}$  and  $r$  lie within the allowed ranges of Eq. (2.10a) and Eq. (2.10c) respectively, whereas  $\alpha_{\text{s}}$  remains quite small. Our numerical results can be interpreted through some simple analytical expressions which are presented in Sec. 3.2.1 [Sec. 3.2.2] for  $n = +1$  [ $n = -1$ ]. There, we also comment on the naturalness of our models, following the arguments of Ref. [6, 7].

#### 3.2.1 NON-MCI WITH $n = +1$

To justify our choice for the negative exponent in Eq. (3.2) we present our formulae below for a general  $n > 0$ . Substituting Eq. (3.2) into Eqs. (2.3) and (2.5) and taking into account that  $c_{\mathcal{R}} \gg 1$ , we obtain

$$J \simeq \sqrt{c_{\mathcal{R}}^n \bar{\sigma}^n}, \quad \widehat{V} = \frac{1}{2} m^2 \sigma^2 \left( 1 + c_{\mathcal{R}} \frac{\sigma}{m_{\text{P}}} \right)^{2n} \simeq \frac{m^2 c_{\mathcal{R}}^{2n} \sigma^{2(1+n)}}{2m_{\text{P}}^{2n}} \quad \text{and} \quad \Gamma_{\sigma} \simeq \frac{1}{192\pi} \frac{m_{\sigma}^3}{m_{\text{P}}^2} \quad (3.7)$$

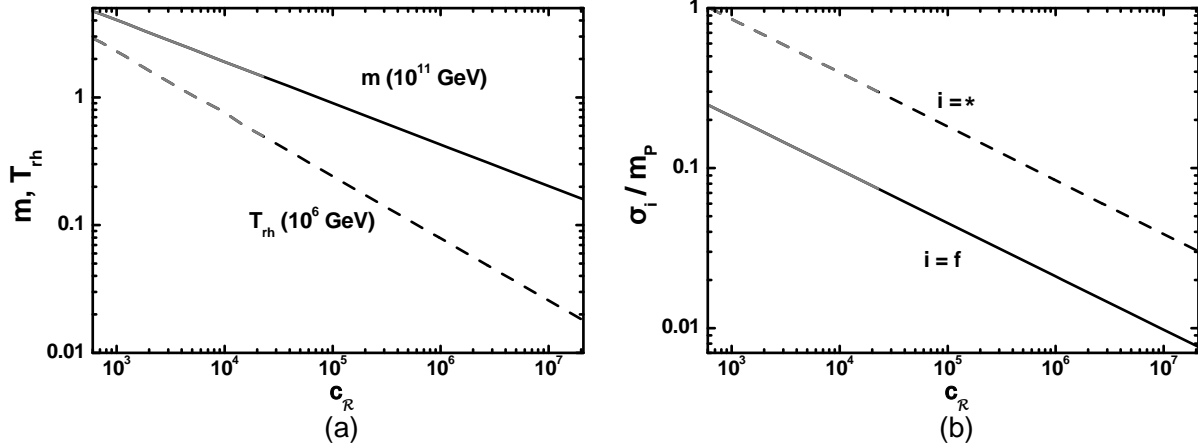


**Figure 1:** The allowed by Eqs. (2.5), (2.6), (2.7) and (2.9) values of  $m$  (solid line) and  $T_{\text{rh}}$  (dashed line) [ $\sigma_f$  (solid line) and  $\sigma_*$  (dashed line)] versus  $c_{\mathcal{R}}$  for non-MCI with  $n = -1$  (a) [(b)]. The gray segments denote values of the various quantities fulfilling Eq. (2.13b) too.

where  $m_\sigma = m$  and obviously  $\langle \sigma \rangle = 0$ . Upon use of Eqs. (2.8), (2.7) and (3.7), the slow roll parameters and  $\hat{N}_*$  read

$$(a) \hat{\epsilon} \simeq \frac{2(1+n)^2}{c_{\mathcal{R}}^n \bar{\sigma}^{n+2}}, \quad \hat{\eta} \simeq \frac{2(1+n)(1+2n)}{c_{\mathcal{R}}^n \bar{\sigma}^{n+2}} = \frac{(1+2n)}{(1+n)} \hat{\epsilon} \quad \text{and} \quad (b) \hat{N}_* \simeq \frac{c_{\mathcal{R}}^n (\bar{\sigma}_*^{n+2} - \bar{\sigma}_f^{n+2})}{2(1+n)(2+n)}. \quad (3.8)$$

Imposing the condition of Eq. (2.8) and solving then Eq. (3.8b) w.r.t  $\sigma_*$  we arrive at

$$\bar{\sigma}_f \simeq (2(1+2n)(1+n)/c_{\mathcal{R}}^n)^{1/(n+2)} \quad \text{and} \quad \bar{\sigma}_* \simeq \left(2(1+n)(2+n)\hat{N}_*/c_{\mathcal{R}}^n\right)^{1/(n+2)}. \quad (3.9)$$

Inserting the last results into Eq. (3.8a), we find through Eq. (2.11)

$$(a) n_s \simeq 1 - 3\hat{\epsilon}_* = 1 - 3(1+n)/(2+n)\hat{N}_* \quad \text{and} \quad (b) r \simeq 16(1+n)/(2+n)\hat{N}_*. \quad (3.10)$$

Letting  $c_{\mathcal{R}}$  vary within its allowed region for  $n = +1$  – see Fig. 1 – we find  $n_s \simeq (0.952 - 0.955)$  and  $r \simeq (0.2 - 0.22)$ . Clearly, increasing  $n$  leads  $r$  above the range of Eq. (2.10c). Therefore, we hereafter concentrate on  $n = +1$  which assures an observationally safe and, at the same time, exciting  $r$ .

Comparing our findings with those obtained for MCI – see Table 1 – we notice that the resulting here  $n_s$ 's are a little lower, whereas  $r$  is significantly elevated and can be probed in the near future from the measurements of PLANCK satellite [35]. Note, in passing, that the so-called Lyth bound [36] on the  $\sigma$  variation,  $\Delta\sigma$ , gets modified within non-MI. Namely, combining Eqs. (2.7) and (2.8) we find

$$\frac{d\sigma}{d\hat{N}} = \sqrt{\frac{r}{8}} \frac{m_{\text{P}}}{J} \Rightarrow \Delta\sigma = \sqrt{\frac{r}{8}} \frac{m_{\text{P}}}{J} \Delta\hat{N} \Rightarrow \Delta\sigma \gtrsim \sqrt{2r} \frac{m_{\text{P}}}{J} \simeq (2.5 - 0.083) m_{\text{P}}/100, \quad (3.11)$$

taking [36]  $\Delta\hat{N} \simeq \Delta N = 4$  and assuming negligible variation of  $f(\sigma)$  from its value at  $\sigma = \sigma_*$ . Therefore, large  $r$ 's do not correlate necessarily with trans-Planckian  $\Delta\sigma$ 's within non-MI. On the other hand,  $\hat{\sigma}$  as evaluated from Eq. (2.3),  $\hat{\sigma} \simeq \sqrt{c_{\mathcal{R}}\sigma^3/m_{\text{P}}}$ , remains trans-Planckian.

The resulting  $\hat{V}$  in Eq. (3.7) is non-renormalizable and suggests that the theory breaks down for energies of the order  $\Lambda = m_{\text{P}}/c_{\mathcal{R}}$ . Checking the consistency with Eq. (2.13a) we find numerically:

$$0.03 \lesssim \hat{H}_*/\Lambda \lesssim 1 \quad \text{for} \quad 625 \lesssim c_{\mathcal{R}} \lesssim 2.26 \cdot 10^4 \quad \text{and} \quad 1 \gtrsim \bar{\sigma}_* \gtrsim 0.3, \quad (3.12)$$

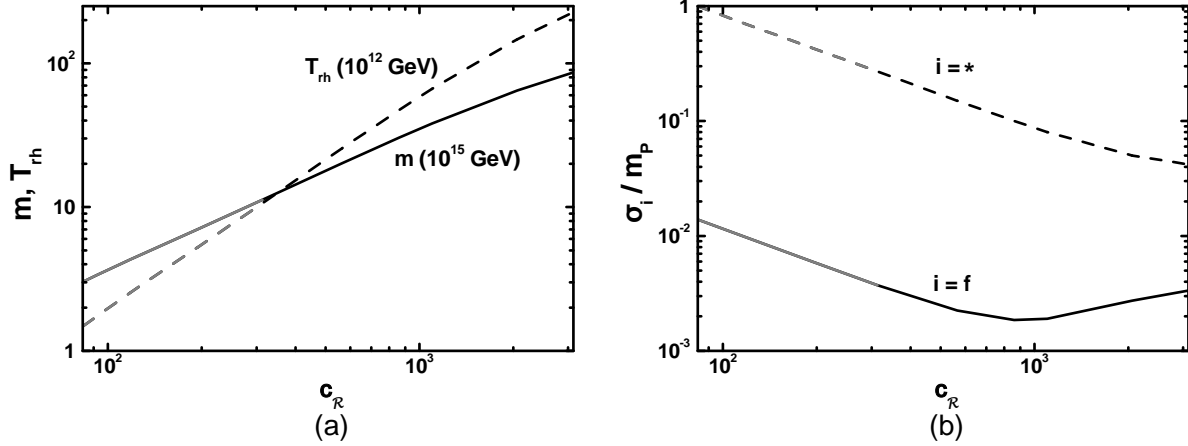


**Figure 2:** The same as in Fig. 1 but for  $n = -1$ . The gray segments here denote values of the various quantities fulfilling Eq. (2.13a) too.

where the corresponding ranges of values are depicted by the gray segments of the lines in Fig. 1. The range in Eq. (3.12) turns out to be a little more comfortable than the one we get within SM non-MI – c.f. Ref. [6]. However, Eq. (2.13a) is violated, since  $\widehat{V}(\sigma_*)^{1/4}/\Lambda \gtrsim 5.8$ .

On the other hand, non-renormalizable terms in the action of Eq. (2.1) and (2.4) indicate that  $\Lambda = m_{\text{P}}$ . In fact, such terms arise from the first term in Eq. (2.1) and the second one in Eq. (2.3). The form of these terms is generated expanding the relevant coefficients in series around  $\sigma = \sigma_*$  with the following result – an expansion in the small field limit,  $c_{\mathcal{R}}\bar{\sigma} \ll 1$ , fails to reproduce the exact results:

$$m_{\text{P}}^2 f \mathcal{R} \ni \frac{m_{\text{P}}}{c_{\mathcal{R}}\bar{\sigma}_*} \left( 1 - 3\frac{\bar{\sigma}}{\bar{\sigma}_*} + 10\left(\frac{\bar{\sigma}}{\bar{\sigma}_*}\right)^2 + \dots \right) \partial^{\bar{\mu}} \partial_{\bar{\mu}} h^{\mu\nu} \quad (3.13a)$$

$$\text{and } m_{\text{P}}^2 \frac{f_{,\sigma}^2}{f^2} \widehat{g}^{\mu\nu} \partial_{\mu} \sigma \partial_{\nu} \sigma \ni \frac{1}{\bar{\sigma}_*^2} \left( 1 - 8\frac{\bar{\sigma}}{\bar{\sigma}_*} + 45\left(\frac{\bar{\sigma}}{\bar{\sigma}_*}\right)^2 + \dots \right) \widehat{g}^{\mu\nu} \partial_{\mu} \sigma \partial_{\nu} \sigma, \quad (3.13b)$$

where  $h^{\mu\nu}$  denotes the graviton field involved in the expansion [6,7] of the metric  $g_{\mu\nu} \simeq \eta_{\mu\nu} + h_{\mu\nu}/m_{\text{P}}$  around the Minkowski space with metric  $\eta_{\mu\nu}$  and  $\mathcal{R}$  is approximated linearly. Given these ambiguities, we do not consider Eq. (3.12a)s absolute constraint.

### 3.2.2 NON-MCI WITH $n = -1$

A completely different situation from that studied in Sec. 3.2.1 emerges for  $n = -1$  in Eq. (3.2). Indeed, substituting Eq. (3.2) into Eqs. (2.3) and (2.5) and taking into account that  $c_{\mathcal{R}} \gg 1$ , we obtain

$$J \simeq \sqrt{3/2} \bar{\sigma}^{-1}, \quad \widehat{V} \simeq \frac{m^2 m_{\text{P}}^2}{2c_{\mathcal{R}}^2} \quad \text{and} \quad \Gamma_{\sigma} \simeq \frac{1}{192\pi} \frac{m_{\sigma}^3}{m_{\text{P}}^2} \quad (3.14)$$

where  $m_{\sigma} = m$  and obviously  $\langle \sigma \rangle = 0$ . We observe that  $\widehat{V}$  exhibits a flat plateau as we obtain for the quartic potential with the standard non-minimal  $f(\sigma)$  – c.f. Ref. [2–4, 34]. Employing Eqs. (2.8), (2.7) and (3.14), the slow roll parameters and  $\widehat{N}_*$  read

$$\text{(a) } \widehat{\epsilon} \simeq \frac{4}{3c_{\mathcal{R}}^2 \bar{\sigma}^2}, \quad \widehat{\eta} \simeq -\frac{4}{3c_{\mathcal{R}} \bar{\sigma}} = -\widehat{\epsilon} c_{\mathcal{R}} \bar{\sigma} \gg -\epsilon \quad \text{and} \quad \text{(b) } \widehat{N}_* \simeq \frac{3c_{\mathcal{R}}}{4} (\bar{\sigma}_* - \bar{\sigma}_{\text{f}}). \quad (3.15)$$

As opposed to our findings in Eqs. (3.3) and (3.8), notice that  $\eta < 0$  here. Imposing the condition of Eq. (2.8) and solving then Eq. (3.15b) w.r.t  $\sigma_*$  we arrive at

$$\bar{\sigma}_{\text{f}} \simeq 2/\sqrt{3}c_{\mathcal{R}} \quad \text{and} \quad \bar{\sigma}_* \simeq 4\widehat{N}_*/3c_{\mathcal{R}}. \quad (3.16)$$

Inserting the last results into Eq. (3.15a), we find through Eq. (2.11)

$$(a) \ n_s \simeq 1 + 2\hat{\eta}_* = 1 - 2/\hat{N}_* \simeq (0.967 - 0.97) \quad \text{and} \quad (b) \ r \simeq 12/\hat{N}_*^2 \simeq (0.002 - 0.003), \quad (3.17)$$

where the ranges above are derived numerically letting  $c_{\mathcal{R}}$  vary within its allowed region – see Fig. 2. Notice that the resulting  $n_s$ 's and  $r$ 's are identical to those derived in Ref. [2, 4]. Comparing them with those listed in Table 1 or given in the paragraph below Eq. (3.10) we remark that  $r$  is significantly reduced, whereas  $n_s$  is close to the value obtained in MCI and a bit larger than the one extracted for non-MCI with  $n = +1$ .

As for the latter case, non-renormalizable terms in the action of Eq. (2.1) indicate an effective cutoff  $\Lambda = m_{\text{P}}/c_{\mathcal{R}}$ , since

$$m_{\text{P}}^2 f_{\mathcal{R}} \ni \frac{c_{\mathcal{R}}}{m_{\text{P}}} \sigma \left( \partial^\mu h_{\mu\bar{\mu}} \partial^\nu h_{\bar{\nu}}^{\bar{\mu}} + \partial^{\bar{\mu}} h_{\mu\nu} \partial^\mu h_{\bar{\mu}\bar{\nu}} + \partial_\mu h \partial^\mu h \right) \quad (3.18)$$

with  $h = h_\mu^\mu = h_{\mu\mu}$ . On the other hand, the second term in Eq. (2.3) gives exactly the same result as in Eq. (3.13b) since  $f_{,\sigma}/f$  is identical for both  $n = \pm 1$  in Eq. (3.2). Checking the consistency with Eq. (2.13a) we find numerically

$$0.3 \lesssim \hat{V}(\sigma_*)^{1/4}/\Lambda \lesssim 1 \quad \text{for} \quad 83 \lesssim c_{\mathcal{R}} \lesssim 313 \quad \text{and} \quad 1 \gtrsim \bar{\sigma}_* \gtrsim 0.27, \quad (3.19)$$

where the corresponding ranges of values are depicted by the gray segments of the lines in Fig. 2. On the other hand, Eq. (2.13b) is satisfied in the whole parameter space of these figures. Consequently, non-MCI with  $n = -1$  can be characterized as more natural than the one with  $n = +1$ .

Concluding this section, let us emphasize that, in contrast to the models suggested in Ref. [20], non-MCI is not of hilltop type and so, complications related to the initial conditions are avoided. Indeed, for non-MCI with  $n = +1$ ,  $\hat{V}$  remains concave upwards, whereas with  $n = -1$ ,  $\hat{V}$  develops a plateau without distinguished maximum. As we explicitly checked, possible inclusion of extra radiative corrections in Eq. (3.1) due to a coupling of  $\sigma$  to fermions – considered in Ref. [20] – do not affect our proposal for values of the relevant Yukawa coupling constant,  $h$ , lower than about  $10^{-3}$ . For such  $h$ 's, the decay width of the inflaton due to this channel dominates over the one given by Eq. (2.5).

## 4 NON-MINIMAL HYBRID INFLATION

Hybrid inflation can be realized in the presence of two real scalar fields,  $\sigma$  and  $\phi$ , involved in the following potential [11]

$$V(\phi, \sigma) = \kappa^2 \left( M^2 - \frac{\phi^2}{4} \right)^2 + \frac{m^2 \sigma^2}{2} + \frac{\lambda^2 \phi^2 \sigma^2}{4}, \quad (4.1)$$

where  $M, m$  are mass parameters and  $\kappa, \lambda$  are dimensionless coupling constants. The global minima of  $V$  lie at  $(\langle \sigma \rangle, \langle \phi \rangle) = (0, \pm 2M)$ . Therefore,  $V$  leads to a spontaneous symmetry breaking of a global or local symmetry depending on the nature of the waterfall field  $\phi$ . In the latter case, topological defects may be also produced via the Kibble mechanism [37]. Trying to keep our approach as simple as possible we below assume that this is not the case.

In addition,  $V$  in Eq. (4.1) gives rise to HI. This is because  $V$  possesses an almost  $\sigma$ -flat direction at  $\phi = 0$  with constant potential density equal to  $V_0 = V(\phi = 0, \sigma) = \kappa^2 M^4$ , for  $m = 0$ . The effective mass squared of the field  $\phi$  along this direction is

$$m_\phi^2 = -\kappa^2 M^2 + \lambda^2 \sigma^2 / 2 > 0 \Leftrightarrow \sigma > \sigma_c = \sqrt{2} \kappa M / \lambda. \quad (4.2)$$

Thus, for  $\sigma > \sigma_c$  the  $\phi = 0$  direction represents a valley of minima which can serve as inflationary trajectory. On this path the potential of HI takes the form

$$V = V_0 + \frac{1}{2}m^2\sigma^2 + V_{\text{rc}} \quad (4.3)$$

where  $V_{\text{rc}}$  is the one-loop correction (to the tree-level potential) which can be written as [21, 23]

$$V_{\text{rc}} = \frac{1}{64\pi^2} \left( m^4 \ln \frac{m^2}{Q^2} + \kappa^2 V_0 (x-1)^2 \ln \frac{\kappa^2 M^2}{Q^2} (x-1) \right) \text{ with } x = \left( \frac{\sigma}{\sigma_c} \right)^2 \quad (4.4a)$$

$$\simeq \frac{\kappa^2 V_0}{64\pi^2} \left( x^2 \ln \frac{\kappa^2 M^2}{Q^2} + \frac{3}{2} \right) \text{ for } x \gg 1. \quad (4.4b)$$

Here,  $Q$  is a renormalization scale which can be conveniently chosen [21] equal to  $\sigma_c$  which practically coincides with the value of  $\sigma$  at the end of HI,  $\sigma_f$ , for both MHI and non-MHI.

We below review (Sec. 4.1) the results for MHI (with  $f(\sigma) = 1$ ) and describe (Sec. 4.2) our findings for non-MHI, seeking the following non-minimal coupling function for the inflaton – for earlier attempts on non-MHI, see Ref. [38]:

$$f(\sigma) = 1 - c_{\mathcal{R}} \bar{\sigma} / (1 + \bar{\sigma})^2 \quad (4.5)$$

where we use, as usually, the shorthand  $\bar{\sigma} = \sigma/m_{\text{P}}$ . As regards the waterfall field we can assume that it is either minimally coupled to gravity or its coupling function is  $f(\phi)$  since  $f(0) = 1$  and  $f(2M) \simeq 1$  for  $c_{\mathcal{R}} \ll 1$  and  $M \leq m_{\text{P}}$ .

#### 4.1 RESULTS FOR MHI

We can get an impression of the expected results for MHI, if we calculate the, involved in the inflationary dynamics, derivatives of  $V$  in Eq. (4.3). Namely we have

$$V_{,\sigma} = m^2\sigma + \frac{x\kappa^2 V_0}{32\pi^2\sigma} (x-1) \left( 2 \ln \frac{\kappa^2 M^2}{Q^2} (x-1) + 1 \right). \quad (4.6)$$

We observe that there are two contributions in  $V_{,\sigma}$ . The first one arises from the tree-level potential whereas the second one comes from the radiative corrections in Eq. (4.4a). When the first contribution dominates over the second one, we obtain the well-known tree-level [11] results,  $N_{\text{tr}*}$  and  $\eta_{\text{tr}}$ , for  $N_*$  and  $\eta$  respectively – note that we identify  $\sigma_f$  with  $\sigma_c$ :

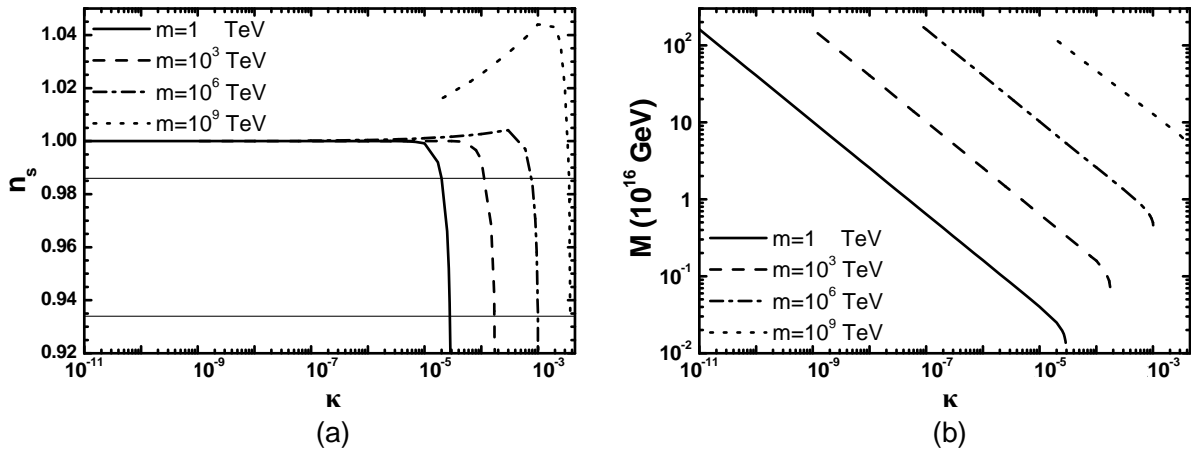
$$N_{\text{tr}*} = \frac{1}{\eta_{\text{tr}}} \ln \frac{\sigma_*}{\sigma_c} \text{ with } \eta_{\text{tr}} = m_{\text{P}}^2 \frac{m^2}{V_0} \gg \epsilon. \quad (4.7)$$

In this regime, the resulting  $n_s$  clearly – see Eq. (2.11) – exceeds slightly unity in contrast to the observationally favored results of Eq. (2.10a). Moreover, as we find numerically, the lower  $\kappa$  and/or  $m$  we use, the closer  $\sigma_*$  is set to  $\sigma_c$ . This is the first kind of tuning occurred within MHI.

Nonetheless, taking into account that the logarithm in Eq. (4.6) turns out to be negative, we can show that, for every  $m$ , there is  $\kappa$  such that  $V$  develops a maximum at  $\sigma = \sigma_{\text{max}}$ , which can be estimated by numerically solving the condition  $V_{,\sigma}(\sigma_{\text{max}}) = 0$ . At  $\sigma = \sigma_{\text{max}}$ ,  $V_{,\sigma\sigma}$  given by

$$V_{,\sigma\sigma} = \frac{V_{,\sigma}}{\sigma} + \frac{x^2\kappa^2 V_0}{16\pi^2\sigma^2} \left( 2 \ln \frac{\kappa^2 M^2}{Q^2} (x-1) + 3 \right), \quad (4.8)$$

becomes negative and so,  $\eta$  and  $n_s$  start decreasing for  $\sigma_*$  close  $\sigma_{\text{max}}$  – see Eqs. (2.8) and (2.11). As for any model of hilltop inflation, the lower  $n_s$  we obtain, the closer  $\sigma_*$  is located to  $\sigma_{\text{max}}$ . This is



$m$ (TeV)	$\kappa$ ( $10^{-3}$ )	$M$ ( $10^{16}$ GeV)	$\Delta_{c*}$	$\Delta_{m*}$
1	0.02 – 0.028	0.025 – 0.015	0.00016 – 0.00029	0.0004 – 0.00007
$10^3$	0.12 – 0.17	0.13 – 0.083	0.0053 – 0.01	0.013 – 0.0023
$10^6$	0.8 – 1	0.69 – 0.49	0.18 – 0.31	0.19 – 0.054
$10^9$	3.55 – 3.72	5.98 – 5.5	4.4 – 5.7	0.38 – 0.24

**Figure 3:** The allowed by Eqs. (2.6), (2.7) and (2.9) values of  $n_s$  (a) and  $M$  (b) versus  $\kappa$  for MHI with  $T_{\text{rh}} = 10^{10}$  GeV,  $\kappa = \lambda$  and several  $m$ 's indicated in the graphs. Shown are also in the table the allowed ranges of the various parameters for  $n_s$  in the range of Eq. (2.10a) limited by thin lines (a).

a second kind of tuning which remains even for non-MHI – see Sec. 4.2. To quantify somehow the amount of the tunings encountered in the considered model, we define the quantities:

$$(a) \Delta_{m*} = \frac{\sigma_{\text{max}} - \sigma_*}{\sigma_{\text{max}}} \quad \text{and} \quad (b) \Delta_{c*} = \frac{\sigma_* - \sigma_c}{\sigma_c}. \quad (4.9)$$

The above rough estimations can be verified by our numerical computations. In our code, we use as input parameters  $\kappa$ ,  $\lambda$ ,  $m$ ,  $M$ ,  $\sigma_*$  and  $T_{\text{rh}}$ . In our analysis for MHI, we fix  $T_{\text{rh}} = 10^{10}$  GeV and  $\kappa = \lambda$  – possible variation of these two choices do not modify our conclusions in any essential way. For any chosen  $\kappa$  and  $m$  we then restrict  $M$  and  $\sigma_*$  so as the restrictions (a), (b) and (d) of Sec. 2.2 and Eq. (4.2) are fulfilled. Using Eq. (2.11) we can extract  $n_s$ ,  $\alpha_s$  and  $r$ . Our results are presented in Fig. 3-(a) [Fig. 3-(b)] where we design the allowed values of  $n_s$  [ $M$ ] versus  $\kappa$  for  $m = 1$  TeV (solid line) or  $m = 10^3$  TeV (dashed line) or  $m = 10^6$  TeV (dot-dashed line) or  $m = 10^9$  TeV (dotted line). The region of Eq. (2.10a) is also limited by thin lines. The various lines terminate at low  $\kappa$ 's due to the saturation of Eq. (2.12b) and at large  $\kappa$ 's since the imposed conditions can not be fulfilled.

Clearly, the almost horizontal part of the various lines, which exceeds the observational limits of Eq. (2.10a), in the  $\kappa - n_s$  plane corresponds to the dominance of the tree-level potential. However, for any  $m$  and relatively large  $\kappa$ 's we can obtain acceptable  $n_s$ 's even without inclusion of extra radiative corrections due to a possible coupling of the inflaton to fermions – c.f. Ref. [21]. On the other hand, it is worth emphasizing that the allowed range of  $\kappa$ 's for each  $m$  is severely tuned. Indeed, confining  $n_s$  within the range of Eq. (2.10a) we find the ranges of the parameters listed in the table of Fig. 3. From the outputs there, we also remark that  $\kappa$ 's,  $M$ 's,  $\Delta_{c*}$ 's and  $\Delta_{m*}$ 's increase with  $m$ . Therefore, the natural realization of MHI requires large  $m$ 's. In this case too,  $M$  turns out to be well above its value within the SUSY version HI – c.f. Ref. [15, 16]. Needless to say, finally, that the resulting  $\alpha_s$ 's and  $r$ 's turn out to be vanishingly small and so, uninteresting. In conclusion, MHI (with the minimal possible radiative corrections) is rather disfavored by the current observational data.

## 4.2 RESULTS FOR NON-MHI

From the analysis of MHI we can deduce that reduction of  $n_s$  for a wider range of  $\kappa$ 's can be achieved if the slope of  $V$  becomes steeper. This objective can be achieved if we employ  $f(\sigma)$  given by Eq. (4.5) with  $c_{\mathcal{R}} \ll 1$ . Another possibility would be  $f(\sigma) = \exp(-c_{\mathcal{R}}\bar{\sigma})$  or that of Eq. (3.2) with  $n > 0$  and  $c_{\mathcal{R}} \sim 0.1$ . However, in these cases the resulting  $\sigma_*$  violates the bound of Eq. (2.12b) and therefore, these options are not adoptable. Moreover, imposing on non-MHI with the standard non-minimal  $f(\sigma)$  the constraints (a), (b) and (d) of Sec. 2.2 and Eq. (4.2), we are obliged to use a tiny  $c_{\mathcal{R}} \sim -10^{-3}$ , which has no sizable impact on reducing  $n_s$ . Consequently, this last choice can not become observationally viable, too.

Differentiating Eq. (4.5) w.r.t  $\sigma$ , substituting into Eqs. (2.3) and (2.5) and taking into account that  $c_{\mathcal{R}} \ll 1$ , we obtain

$$f_{,\sigma} = \frac{c_{\mathcal{R}}(-1 + \bar{\sigma})}{m_{\text{P}}(1 + \bar{\sigma})^3}, \quad f_{,\sigma\sigma} = \frac{2c_{\mathcal{R}}(2 - \bar{\sigma})}{m_{\text{P}}^2(1 + \bar{\sigma})^4}, \quad \widehat{V} \simeq V_0, \quad J \simeq 1 \quad \text{and} \quad \Gamma_{\sigma} = \frac{c_{\mathcal{R}}^2}{128\pi} \frac{m_{\sigma}^3}{m_{\text{P}}^2} \quad (4.10)$$

where  $m_{\sigma} = \sqrt{2\lambda^2 M^2 + m^2}$ . Despite the fact that  $\widehat{V}$  given by Eqs. (2.3) and (4.3) is practically equal to  $V_0$  – since  $f(\bar{\sigma}) \simeq 1$  for  $\bar{\sigma} \ll 1$  –, its inclination is mostly dominated by the term  $-2V_0 f_{,\sigma}$  of  $V_{,\sigma}$ . Indeed, upon use of Eqs. (2.8), (4.4b) and (4.10) we find

$$\widehat{\epsilon} = \frac{m_{\text{P}}^2}{2} \left( -2f_{,\sigma} + \frac{m^2\sigma}{V_0} + \frac{\kappa^2 x^2}{16\pi^2 \sigma} \ln \frac{\kappa^2 M^2}{Q^2} \right)^2. \quad (4.11)$$

In a sizable portion of the parameter space, the first contribution to  $\widehat{\epsilon}$  in Eq. (4.11) overshadows the others two. As a consequence,  $\widehat{V}$  develops a maximum at  $\bar{\sigma} = \bar{\sigma}_{\text{max}}$  for  $f_{,\sigma}(\bar{\sigma}_{\text{max}}) = 0 \Leftrightarrow \bar{\sigma}_{\text{max}} \simeq 1$  with  $\widehat{V}_{,\sigma\sigma}(\sigma_{\text{max}}) < 0$ . In fact, inserting Eqs. (2.3) and (4.3) into Eq. (2.8) we end up with

$$\widehat{\eta} = m_{\text{P}}^2 \left( -2f_{,\sigma\sigma} + \frac{m^2}{V_0} + \frac{3\kappa^2 x^2}{16\pi^2 \sigma^2} \ln \frac{\kappa^2 M^2}{Q^2} \right), \quad (4.12)$$

which is negative for dominant  $f_{,\sigma\sigma}$  with  $\bar{\sigma} < 2$ . Combining Eqs. (4.12) with (2.11a) we can easily infer that  $c_{\mathcal{R}} > 0$  for  $\bar{\sigma} < \bar{\sigma}_{\text{max}}$  strengthens significantly the reduction of  $n_s$ . Neglecting the two last terms in the right-hand side of Eq. (4.11), we can estimate  $\widehat{N}_*$  via Eq. (2.7) with result

$$\widehat{N}_* \simeq \frac{1}{2m_{\text{P}}^2} \int_{\sigma_*}^{\sigma_c} \frac{d\sigma}{f_{,\sigma}} = \frac{1}{6c_{\mathcal{R}}} \left( (21 + 6\bar{\sigma}_* + \bar{\sigma}_*^2) \bar{\sigma}_* - (21 + 6\bar{\sigma}_c + \bar{\sigma}_c^2) \bar{\sigma}_c + 24 \ln \frac{1 - \bar{\sigma}_*}{1 - \bar{\sigma}_c} \right). \quad (4.13)$$

As we verify numerically, the formula above gives accurate results for  $m \leq 10^6$  TeV and sufficiently low  $\kappa$ 's. However, since  $\sigma_*$  depends on  $\widehat{N}_*$  in a rather complicate way, it is not doable to find an analytical result for  $n_s$  as a function of  $\widehat{N}_*$  – c.f. Eq. (3.9) and Eq. (3.9). Therefore, our last resort is the numerical computation, whose the results are presented in the following.

In our code, we use as input parameters  $\kappa$ ,  $\lambda$ ,  $m$ ,  $M$ ,  $\sigma_*$  and  $c_{\mathcal{R}}$ . Note that  $T_{\text{rh}}$  is calculated via Eq. (2.5). For every chosen  $\kappa$ ,  $\lambda$ ,  $m$  and  $c_{\mathcal{R}}$ , we can restrict  $M$  and  $\sigma_*$  so as the conditions (a), (b) and (d) of Sec. 2.2 and Eq. (4.2) are fulfilled. Through Eq. (2.11) we can then extract  $n_s$  and  $\alpha_s$ . Following this strategy, in Fig. 4-(a) [Fig. 4-(b)] we display the allowed values of  $n_s$  [ $M$ ] versus  $c_{\mathcal{R}}$  with  $m \leq 10^6$  TeV,  $\kappa = 10^{-5}$  and  $\lambda = \kappa$  (solid lines)  $\lambda = 5\kappa$  (dashed lines) and  $\lambda = 0.5\kappa$  (dotted lines). The region of Eq. (2.10a) is also limited by thin lines. We observe that as  $c_{\mathcal{R}}$  increases,  $n_s$  decreases entering the observationally favored region of Eq. (2.10a). On the other hand,  $M$  increases with  $c_{\mathcal{R}}$  until a certain  $c_{\mathcal{R}} \simeq 0.03 - 0.05$  and then decreases. Surprisingly the value of  $c_{\mathcal{R}}$ , at which the maximum  $M$  is encountered, corresponds more or less to the central observational  $n_s \simeq 0.96$ . We also observe that increasing  $\lambda$  above  $\kappa$  with fixed  $c_{\mathcal{R}}$ ,  $n_s$  drops but  $M$  raises. These results can be

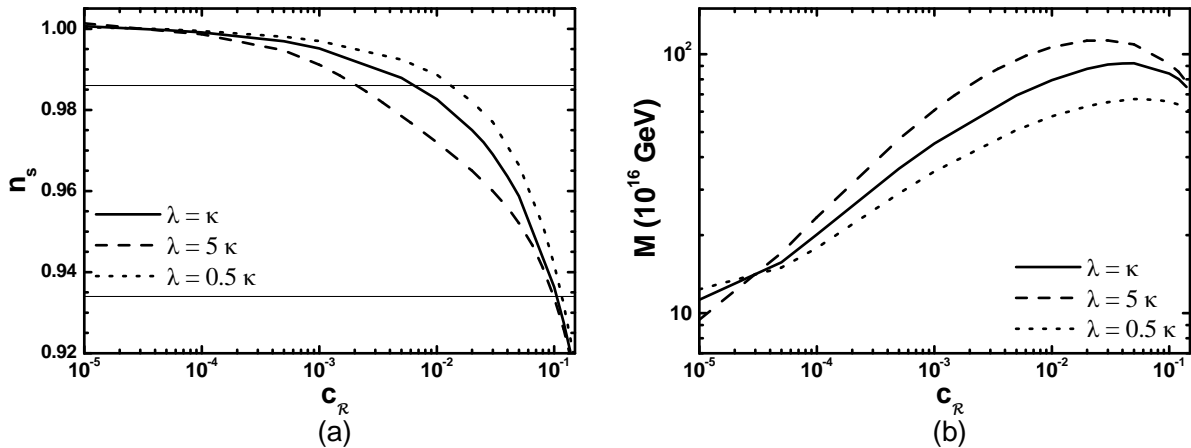


**Figure 4:** The allowed by Eqs. (2.6), (2.7) and (2.9) – with  $T_{\text{rh}}$  given by Eq. (2.5) – values of  $n_s$  (a) and  $M$  (b) versus  $c_{\mathcal{R}}$  for non-MHI with  $m \leq 10^6$  TeV,  $\kappa = 10^{-5}$  and several  $\lambda$ 's indicated in the graphs. The region of Eq. (2.10a) is also limited by thin lines.

understood as follows: As  $\lambda/\kappa$  elevates  $\sigma_c$  decreases – see Eq. (4.2) – and therefore,  $\sigma_*$  decreases, with fixed  $\widehat{N}_*$ . This effect causes an increase of  $|f_{,\sigma}(\sigma_*)|$  and  $f_{,\sigma\sigma}(\sigma_*)$  – see Eq. (4.10). As a consequence,  $M$  increases too, since  $M$  is proportional to  $f_{,\sigma}^{1/2}$  due to Eq. (2.6). Also,  $|\eta|$  increases – according to Eq. (4.12) – and so,  $n_s$  drops efficiently – see Eq. (2.11).

Confronting non-MHI with all the constraints of Sec. 2.2 consistently with Eq. (4.2), we can delineate the allowed (lightly gray shaded) regions in the  $\kappa - c_{\mathcal{R}}$  [ $\kappa - M$ ] plane as in Fig. 5-(a<sub>1</sub>), (b<sub>1</sub>) and (c<sub>1</sub>) [Fig. 5-(a<sub>2</sub>), (b<sub>2</sub>) and (c<sub>2</sub>)]. In Fig. 5-(a<sub>1</sub>) and (a<sub>2</sub>) we take  $\lambda = \kappa$ . Our results for this choice are  $m$ -independent for any  $\kappa$  and  $m \leq 10^6$  TeV. On the other hand, in Fig. 5-(b<sub>1</sub>) and (b<sub>2</sub>) [Fig. 5-(c<sub>1</sub>) and (c<sub>2</sub>)] we set  $\lambda = 5\kappa$  and  $m = 10^8$  TeV and [ $\lambda = 0.5\kappa$  and  $m = 10^7$  TeV]. The conventions adopted for the various lines are also shown in the left-hand side of each graph. In particular, the gray dot-dashed [dashed] lines correspond to  $n_s = 0.986$  [ $n_s = 0.934$ ], whereas the gray solid lines have been obtained by fixing  $n_s = 0.96$  – see Eq. (2.10). For  $\kappa$ 's below the solid black line, our initial requirement in Eq. (2.12b) is violated. For  $\kappa$ 's larger than those depicted in the graphs we do not find solutions consistent with the imposed restrictions of Sec. 2.2. The upper bounds of the allowed regions in the  $\kappa - M$  plane come from  $c_{\mathcal{R}}$  leading to  $n_s = 0.96$  – see Fig. 4-(b). Although this result may not rigorously correct, it is accurate enough for our pictorial purposes. In all cases, the allowed ranges of  $\kappa$ 's – although restricted to values lower than 0.001 – are much more wide and natural than the ones obtained for MHI – c.f. Table of Fig. 3. Confining  $n_s$  to its central observational value, we obtain the ranges of the various parameters arranged in the Table of Fig. 5. We observe there that, for fixed  $n_s$  and increasing  $\kappa$ ,  $c_{\mathcal{R}}$  and  $M$  decrease whereas  $\Delta_{c^*}$  and  $\Delta_{m^*}$  increase. As a consequence, for any  $m$ , the tuning regarding  $\Delta_{c^*}$  is greatly alleviated compared to the outputs of MHI, whereas we are let with the usual mild tuning required for  $\Delta_{m^*}$ . This is present to any inflationary hilltop model – c.f. Ref. [16]. The allowed  $M$ 's mostly exceed the SUSY grand unification scale,  $M_{\text{GUT}} \simeq 2.86 \cdot 10^{16}$  GeV, whereas  $T_{\text{rh}}$  mostly increases with  $\kappa$ , as can be noticed via Eqs. (2.5) and (4.10).

From our findings, we can conclude that: (i) the required  $c_{\mathcal{R}}$ 's are rather low and so, complications related to the hierarchy between the inflationary scale and the effective cutoff of the theory are avoided; (ii) our results depend rather weakly on the variation of  $m$ , for  $m \leq 5 \cdot 10^8$  TeV; (iii) as  $m$  raises above  $5 \cdot 10^8$  TeV and  $\kappa$  drops below 0.001, Eq. (2.12b) is eventually violated and so, our scheme becomes unapplicable; (iv) similarly to MHI,  $\alpha_s$  and  $r$  turn out to be negligibly small.

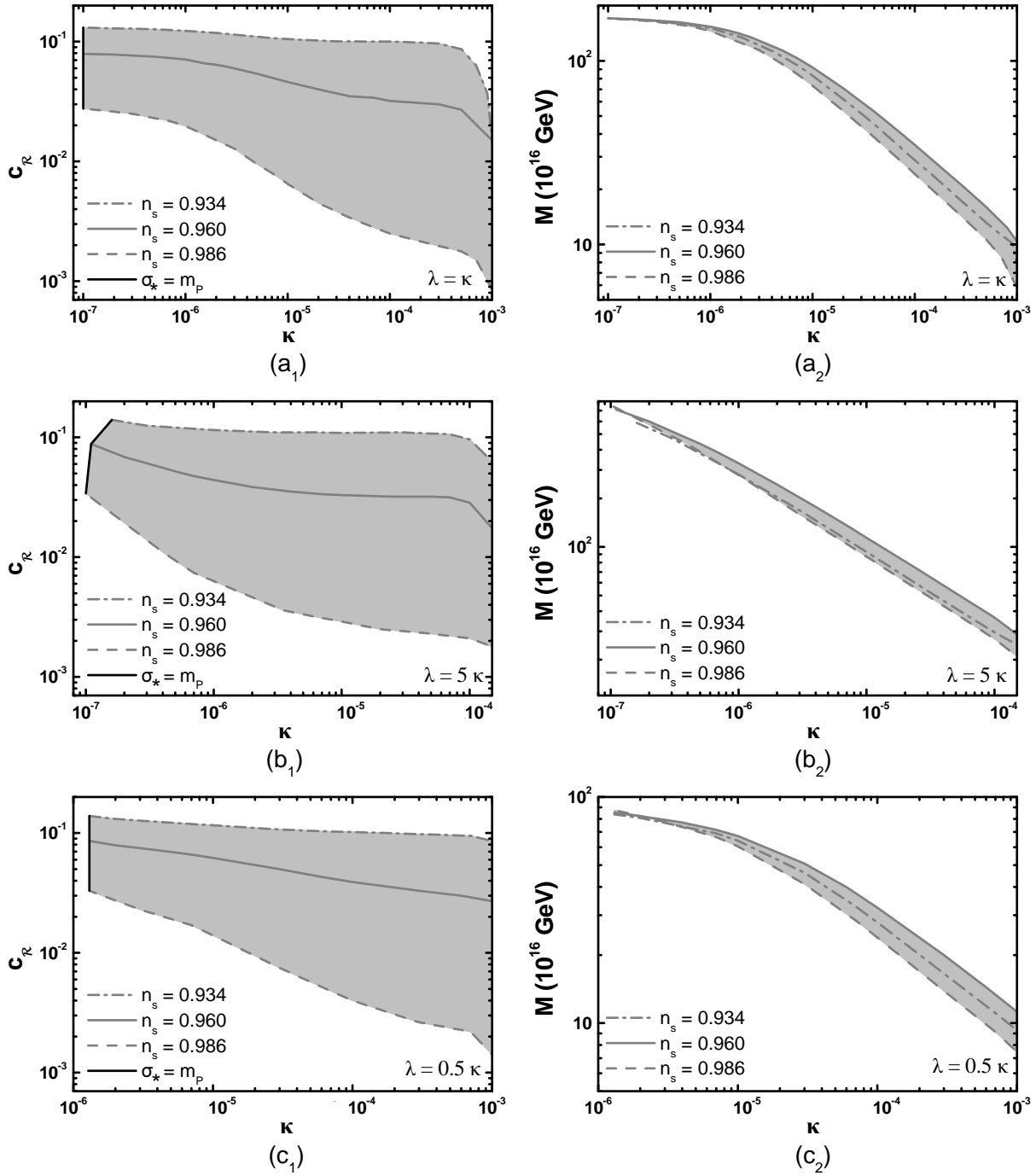


Fig.	$\kappa/10^{-3}$	$c_{\mathcal{R}}/10^{-2}$	$M/10^{16}$ GeV	$T_{\text{rh}}/10^8$ GeV	$\Delta_{c^*}$	$\Delta_{m^*}/10^{-2}$
(a <sub>1</sub> ), (a <sub>2</sub> )	0.0002 – 1	7.8 – 1.5	168 – 10	0.0028 – 3.5	0.016 – 7	0.91 – 31
(b <sub>1</sub> ), (b <sub>2</sub> )	0.00011 – 0.2	8.8 – 1.8	711 – 25	0.12 – 13	0.21 – 18	9.6 – 32
(c <sub>1</sub> ), (c <sub>2</sub> )	0.0013 – 1	8.6 – 2.7	85 – 11	0.006 – 2.1	0.03 – 4	1.5 – 32

**Figure 5:** Allowed (lightly gray shaded) by the restrictions of Sec. 2.2 areas in the  $\kappa - c_{\mathcal{R}}$  [ $\kappa - M$ ] plane (a<sub>1</sub>, b<sub>1</sub> and c<sub>1</sub>) [(a<sub>2</sub> b<sub>2</sub> and c<sub>2</sub>)] for non-MHI. We take  $\kappa = \lambda$  and  $m \leq 10^6$  TeV (a<sub>1</sub> and a<sub>2</sub>) or  $m = 10^8$  TeV and  $\lambda = 5\kappa$  (b<sub>1</sub> and b<sub>2</sub>) or  $m = 10^7$  TeV and  $\lambda = 0.5\kappa$  (c<sub>1</sub> and c<sub>2</sub>). The conventions adopted for the various lines are also shown. The allowed ranges of the various parameters for  $n_s = 0.96$  are listed in the table.

As in the case of non-MCI, our proposal remains intact even if we add fermion-dominated one-loop radiative corrections in Eq. (4.3) – c.f. Ref. [21] – provided the values of the relevant Yukawa coupling constant,  $h$ , remains lower than about  $10^{-4}$ . For  $h$ 's close to this value, the decay width of the inflaton, due to this channel dominates over the one given by Eq. (2.5).

## 5 CONCLUSIONS

We considered the non-SUSY version of CI (driven by quadratic potential) and HI, assuming a non-minimal coupling function,  $f(\sigma)$ , between the inflaton field and the Ricci scalar curvature. Using the freedom of choosing this scalar function, we deliberated CI from the problem of trans-Planckian inflaton values and achieved observationally acceptable  $n_s$ 's for a wide range of the parameters of HI. As a bonus, the selected  $f(\sigma)$ 's give rise to Yukawa-type interactions between the inflaton and matter fields leading to a successful post-inflationary reheating. Afterwards, the proposed  $f(\sigma)$ 's reduce to unity and so, the Einstein gravity is naturally recovered.

Specifically, the adopted forms of  $f(\sigma)$  are given by Eq. (3.2) and Eq. (4.5) for non-MCI and non-MHI, respectively. In both cases, the parameter  $c_{\mathcal{R}}$  involved in  $f(\sigma)$  can be constrained so as the results of the inflationary models can be reconciled with a number of theoretical and observational restrictions. Our results are as follows:

- In the case of non-MCI, we find  $625 \lesssim c_{\mathcal{R}} \lesssim 2.1 \cdot 10^7$  resulting to  $n_s \simeq 0.955$  and  $r \simeq (0.2-0.22)$  for  $n = +1$  and  $83 \lesssim c_{\mathcal{R}} \lesssim 3120$  resulting to  $n_s \simeq 0.967$  and  $r \simeq (0.002 - 0.003)$  for  $n = -1$ . In sharp contrast to MCI, only sub-Planckian values of the inflaton field in the Jordan frame are utilized avoiding, thereby, destabilization of the inflationary scenarios from possible corrections caused by quantum gravity. Comments on the naturalness of the models are also given.
- In the case of non-MHI, the chosen  $f(\sigma)$  leads to hilltop-type inflation for a wide range for  $\kappa$ 's. As a consequence, observationally acceptable results require a proximity between the values of the inflaton field at the maximum of the potential and at the horizon crossing of the pivot scale. The amount of this tuning was measured by the quantity  $\Delta_{m^*}$  defined in Eq. (4.9b). E.g., for  $m \leq 10^6$  TeV and the observationally central value of  $n_s$ , we find  $c_{\mathcal{R}} \simeq (0.015 - 0.078)$  with  $M \simeq (1 - 16.8) \cdot 10^{17}$  GeV,  $\lambda = \kappa \simeq (2 \cdot 10^{-7} - 0.001)$  and  $\Delta_{m^*} \simeq (0.91 - 32)\%$ . Compared to MHI, we find that the observational requirements can be satisfied without tuning severely neither  $\kappa$  nor  $\Delta_{c^*}$  defined in Eq. (4.9a) even for low  $m$ 's – see Tables of Figs. 3 and 5. Therefore, the proposed non-MHI is more favored by the current data.

We explicitly checked that, for both models of non-MI, the proposed scheme remains valid even if an extra coupling of the inflaton to fermions exists, provided that the relevant coupling constant is somewhat suppressed. If these fermions are identified with right-handed neutrinos, baryogenesis via non-thermal leptogenesis [39] is, in principle, possible – in the case of HI, baryogenesis can be also accomplished if only the waterfall field is coupled to right-handed neutrinos. Note that, in our framework, the decay of the inflaton to right-handed neutrinos is also possible due to curvature-induced [24] couplings. However, the resulting decay width is reduced [24] compared to this given by Eq. (2.5) and so, the produced lepton asymmetry is lower than the expectations for all possible masses of right-handed neutrinos. On the other hand, since baryogenesis can be realized in a variety of ways – see, e.g., Ref. [25, 40] – we opted not to complicate our presentation with secondary mechanisms which may or may not affect the inflationary observable quantities.

It would be interesting to investigate if a similar realization of non-MI can be accomplished in the framework of SUGRA, along the lines of Ref. [41]. In such a case, the inflaton of non-MCI could be identified with one of the right-handed sneutrinos. On the other hand, a possible SUSY version [15, 16] of non-MHI could become compatible with larger (and more natural) values of the relevant coupling constant  $\kappa = \lambda$ .

## REFERENCES

- [1] K. Nozari and S.D. Sadatian, *Mod. Phys. Lett. A* **23**, 2933 (2008) [arXiv:0710.0058];  
K. Nozari and S. Shafizadeh, *Phys. Scripta* **82**, 015901 (2010) [arXiv:1006.1027];
- [2] F.L. Bezrukov and M. Shaposhnikov, *Phys. Lett. B* **659**, 703 (2008) [arXiv:0710.3755];  
A.O. Barvinsky *et al.*, *J. Cosmol. Astropart. Phys.* **11**, 021 (2008) [arXiv:0809.2104];  
N. Okada, M. Ur Rehman and Q. Shafi, arXiv:0911.5073.
- [3] S.C. Park and S. Yamaguchi, *J. Cosmol. Astropart. Phys.* **08**, 009 (2008) [arXiv:0801.1722].
- [4] A. De Simone, M.P. Hertzberg and F. Wilczek, *Phys. Lett. B* **678**, 1 (2009) [arXiv:0812.4946].
- [5] T.E. Clark, B. Liu, S.T. Love and T. ter Veldhuis, *Phys. Rev. D* **80**, 075019 (2009) [arXiv:0906.5595];  
R.N. Lerner and J. McDonald, *Phys. Rev. D* **80**, 123507 (2009) [arXiv:0909.0520].
- [6] C.P. Burgess, H.M. Lee and M. Trott, *J. High Energy Phys.* **09**, 103 (2009) [arXiv:0902.4465];  
J.L.F. Barbon and J.R. Espinosa, *Phys. Rev. D* **79**, 081302 (2009) [arXiv:0903.0355];  
C.P. Burgess, H.M. Lee and M. Trott, arXiv:1002.2730;  
M.P. Hertzberg, arXiv:1002.2995.
- [7] R.N. Lerner and J. McDonald, *J. Cosmol. Astropart. Phys.* **04**, 015 (2010) [arXiv:0912.5463].
- [8] E. Elizalde *et al.*, *Phys. Rev. D* **77**, 106005 (2008) [arXiv:0803.1311].
- [9] D.H. Lyth and A. Riotto, *Phys. Rept.* **314**, 1 (1999) [hep-ph/9807278];  
A. Mazumdar and J. Rocher, arXiv:1001.0993.
- [10] A.D. Linde, *Phys. Lett. B* **129**, 177 (1983).
- [11] A.D. Linde, *Phys. Rev. D* **49**, 748 (1994);  
E.J. Copeland *et al.*, *Phys. Rev. D* **49**, 6410 (1994) [astro-ph/9401011].
- [12] E. Komatsu *et al.* [WMAP Collaboration], *Astrophys. J. Suppl.* **180**, 330 (2009) [arXiv:0803.0547];  
E. Komatsu *et al.* [WMAP Collaboration], arXiv:1001.4538  
<http://lambda.gsfc.nasa.gov/product/map/dr2/parameters.cfm>
- [13] S. Clesse and J. Rocher, *Phys. Rev. D* **79**, 103507 (2009) [arXiv:0809.4355].
- [14] M. Kawasaki, M. Yamaguchi and T. Yanagida, *Phys. Rev. Lett.* **85**, 3572 (2000) [hep-ph/0004243];  
M.C. Bento, R.G. Felipe and N.M.C. Santos, *Phys. Rev. D* **69**, 123513 (2004) [hep-ph/0402276];  
M. Bastero-Gil and A. Berera, *Phys. Rev. D* **71**, 063515 (2005) [hep-ph/0507124];  
S. Dimopoulos *et al.*, *J. Cosmol. Astropart. Phys.* **08**, 003 (2008) [hep-th/0507205].
- [15] G.R. Dvali, Q. Shafi and R.K. Schaefer, *Phys. Rev. Lett.* **73**, 1886 (1994) [hep-ph/9406319].
- [16] M. Bastero-Gil, S.F. King and Q. Shafi, *Phys. Lett. B* **651**, 345 (2007) [hep-ph/0604198];  
B. Garbrecht, C. Pallis and A. Pilaftsis, *J. High Energy Phys.* **12**, 038 (2006) [hep-ph/0605264];  
M. Ur Rehman, V.N. Şenoğuz and Q. Shafi, *Phys. Rev. D* **75**, 043522 (2007) [hep-ph/0612023];  
C. Pallis, *J. Cosmol. Astropart. Phys.* **04**, 024 (2009) [arXiv:0902.0334];  
M. Ur Rehman, Q. Shafi and J.R. Wickman, *Phys. Lett. B* **683**, 191 (2010) [arXiv:0908.3896];  
M. Ur Rehman, Q. Shafi and J.R. Wickman, *Phys. Lett. B* **688**, 75 (2010) [arXiv:0912.4737].
- [17] R.A. Battye, B. Garbrecht and A. Moss, *J. Cosmol. Astropart. Phys.* **09**, 007 (2006) [astro-ph/0607339];  
R.A. Battye, B. Garbrecht and A. Moss, *Phys. Rev. D* **81**, 123512 (2010) [arXiv:1001.0769].
- [18] G. Lazarides and C. Pallis, *Phys. Lett. B* **651**, 216 (2007) [hep-ph/0702260];  
G. Lazarides, *Int. J. Mod. Phys. A* **22**, 5747 (2007) [arXiv:0706.1436];  
C. Pallis, *AIP Conf. Proc.* **1122**, 368 (2009) [arXiv:0812.0249];  
G. Lazarides and C. Pallis, arXiv:1007.1558.
- [19] C. Pallis, "High Energy Physics Research Advances", edited by T.P. Harrison and R.N. Gonzales (Nova Science Publishers Inc., New York, 2008) [arXiv:0710.3074].
- [20] V.N. Şenoğuz and Q. Shafi, *Phys. Lett. B* **668**, 6 (2008) [arXiv:0806.2798].

- [21] M. Ur Rehman, Q. Shafi and J.R. Wickman, *Phys. Rev. D* **79**, 103503 (2009) [arXiv:0901.4345].
- [22] L. Boubekeur and D. Lyth, *J. Cosmol. Astropart. Phys.* **07**, 010 (2005) [hep-ph/0502047];  
K. Kohri, C.M. Lin and D.H. Lyth, *J. Cosmol. Astropart. Phys.* **12**, 004 (2007) [arXiv:0707.3826];  
C.M. Lin and K. Cheung, *J. Cosmol. Astropart. Phys.* **03**, 012 (2009) [arXiv:0812.2731].
- [23] S.R. Coleman and E.J. Weinberg, *Phys. Rev. D* **7**, 1888 (1973).
- [24] Y. Watanabe and E. Komatsu, *Phys. Rev. D* **75**, 061301 (2007) [gr-qc/0612120];  
Y. Watanabe and E. Komatsu, *Phys. Rev. D* **77**, 043514 (2008) [arXiv:0711.3442].
- [25] E.W. Kolb and M.S. Turner, *The Early Universe*, Redwood City, USA: Addison-Wesley (1990).
- [26] K. Maeda, *Phys. Rev. D* **39**, 3159 (1989);  
S. Kalara, N. Kaloper and K.A. Olive, *Nucl. Phys.* **B341**, 252 (1990);  
V. Faraoni, E. Gunzig and P. Nardone, *Fund. Cosmic Phys.* **20**, 121 (1999) [gr-qc/9811047];  
S. Carloni, E. Elizalde and S. Odintsov, arXiv:0907.3941.
- [27] G. Lazarides, *J. Phys. Conf. Ser.* **53**, 528 (2006) [hep-ph/0607032];  
D. Baumann, arXiv:0907.5424.
- [28] D.S. Salopek, J.R. Bond and J.M. Bardeen, *Phys. Rev. D* **40**, 1753 (1989);  
F. Bauer and D.A. Demir, *Phys. Lett. B* **665**, 222 (2008) [arXiv:0803.2664];  
N. Makino and M. Sasaki, *Prog. Theor. Phys.* **86**, 103 (1991);  
R. Fakir, S. Habib and W. Unruh, *Astrophys. J.* **394**, 396 (1992);  
D.I. Kaiser, *Phys. Rev. D* **52**, 4295 (1995) [astro-ph/9408044]  
T. Chiba and M. Yamaguchi, *J. Cosmol. Astropart. Phys.* **10**, 021 (2008) [arXiv:0807.4965].
- [29] C. Pallis, *Nucl. Phys.* **B751**, 129 (2006) [hep-ph/0510234];  
C. Pallis, *Nucl. Phys.* **B831**, 217 (2010) [arXiv:0909.3026].
- [30] N. Sugiyama and T. Futamase, *Phys. Rev. D* **81**, 023504 (2010).
- [31] N. Bartolo, E. Komatsu, S. Matarrese and A. Riotto, *Phys. Rept.* **402**, 103 (2004) [astro-ph/0406398];  
X. Chen, arXiv:1002.1416.
- [32] A.D. Linde, *Particle Physics and Inflationary Cosmology*, Harwood, Chur, Switzerland, (1990) [hep-th/0503203];  
A.D. Linde, *Lect. Notes Phys.* **738**, 1 (2008) [arXiv:0705.0164].
- [33] R. Fakir and W.G. Unruh, *Phys. Rev. D* **41**, 1783 (1990);  
E. Komatsu and T. Futamase, *Phys. Rev. D* **59**, 064029 (1999) [astro-ph/9901127];  
S. Tsujikawa and B. Gumjudpai, *Phys. Rev. D* **69**, 123523 (2004) [astro-ph/0402185].
- [34] N. Okada, M.U. Rehman and Q. Shafi, arXiv:1005.5161;  
N. Okada and Q. Shafi, arXiv:1007.1672.
- [35] <http://www.rssd.esa.int/SA/PLANCK/include/report/redbook/redbook-science.htm>
- [36] D.H. Lyth, *Phys. Rev. Lett.* **78**, 1861 (1997) [hep-ph/9606387];  
R. Easther, W.H. Kinney and B.A. Powell, *J. Cosmol. Astropart. Phys.* **08**, 004 (2006) [astro-ph/0601276].
- [37] T.W.B. Kibble, *J. Phys. A* **9**, 387 (1976).
- [38] V. Faraoni, *Phys. Rev. D* **53**, 6813 (1996) [astro-ph/9602111];  
S. Koh, S.P. Kim and D.J. Song, *Phys. Rev. D* **72**, 043523 (2005) [astro-ph/0505188].
- [39] G. Lazarides and Q. Shafi, *Phys. Lett. B* **258**, 305 (1991);  
G. Lazarides, R.K. Schaefer and Q. Shafi, *Phys. Rev. D* **56**, 1324 (1997) [hep-ph/9608256].
- [40] K. Hamaguchi, *Phd Thesis* [hep-ph/0212305];  
W. Buchmuller, R.D. Peccei and T. Yanagida, *Ann. Rev. Nucl. Part. Sci.* **55**, 311 (2005) [hep-ph/0502169].
- [41] M.B. Einhorn and D.R.T. Jones, *J. High Energy Phys.* **03**, 026 (2010) [arXiv:0912.2718];  
S. Ferrara, R. Kallosh, A. Linde, A. Marrani and A. Van Proeyen, arXiv:1004.0712.